PAPER

Check for updates

Chemical vapor deposition of partially oxidized graphene

Zafer Mutlu,†[a] Isaac Ruiz,†[b] Ryan J. Wu, [ID][c] Robert Ionescu,[a] Sina Shahrezaei,[a] Selcuk Temiz,[a] Mihrimah Ozkan,[b] K. Andre Mkhoyan [ID][c] and Cengiz S. Ozkan [ID] *[ad]

Herein, we report on chemical vapor deposition (CVD) of partially oxidized graphene (POG) films on electropolished polycrystalline copper foils at relatively low temperature under near-atmospheric pressure. The structural, chemical, and electronic properties of the films are studied in detail using several spectroscopic and microscopic techniques. The content of carbon and oxygen in the films is identified by chemical mapping at near-atomic scale. Electron diffraction patterns of the films possess clear diffraction spots with a six-fold pattern that is consistent with the hexagonal lattice. The fine structure of the carbon K-edge signal in STEM-EELS spectra of the films is distinguishable from that of graphene and graphite. The presence of oxygen in the films is further supported by a clear oxygen K-edge. Raman spectroscopy and XPS results provide direct evidence for a lower degree of oxidation. The work function of the films is found to be much higher than that of graphene, using UPS measurements.

Introduction

Graphene oxide (GO), a heavily oxidized derivative of graphene, has recently gained extraordinary attention for its great potential use as an intermediate in the mass production of graphene,[1] and a broad range of applications.[1,2] GO can be visualized as individual sheets of graphene decorated with oxygen functional groups on both basal planes and edges.[3]

GO can be synthesized by various methods, as reported by Staudenmaier,[4] Hofmann,[5] Hummers,[6] and Tour,[7] where bulk graphite is generally chemically oxidized to graphite oxide and then exfoliated to the individual layers of GO. Among these methods, Hummers' method is the most common method used today for mass production of graphene. In Hummers' method, the oxidation of graphite is accomplished by treating graphite with potassium permanganate ($KMnO_4$) and sodium nitrate ($NaNO_3$) in concentrated sulfuric acid (H_2SO_4). The common challenges associated with these GO production routes include chemical inhomogeneity, batch-to-batch reproducibility and generation of defects.[8] The surface properties, structural features, purity, and colloidal dispersity of GO vary substantially depending on the synthesis method used due to the differences in the reaction conditions, type of graphitic material and purification processing used.[9]

Band gap opening and scaling is one of the priorities in the development of graphene-based electronics. GO is an insulator,[10] but controlled removal of oxygen functional groups can transform it to a semiconductor and ultimately to a semi-metal graphene.[11] On the other hand, it is possible to open a band gap in graphene by adding oxygen functional groups onto its surface by plasma treatment.[12,13] Ideally, by controlling the oxidation degree, one can engineer the band gap of graphene. However, oxygen plasma treatment can introduce structural disorders and defects into graphene layers, and suffers from non-uniform functionalization, and additional processing steps, which hinders its potential applications.

Chemical vapor deposition (CVD) has emerged as the most versatile and promising technique to grow graphene[14] and graphene-like 2D materials.[15–18] However, the formation of graphene nucleation with high density on copper (Cu) foils at the initial stage of CVD growth can lead to high-density domain boundaries in graphene films, resulting in severe degradation of its carrier transport properties[19] and mechanical strength.[20] Recently, several research groups[21–25] have reported that treating the surface of Cu foils with oxygen can significantly reduce graphene nucleation density, resulting large graphene domains. While most of the previous research[26] has focused on improving graphene growth using oxygen, less attention[27,28] has been paid to CVD growth of GO and its derivatives using oxygen.

Herein, we have demonstrated CVD growth of partially oxidized graphene (POG) films on electropolished poly-crystalline Cu foils, treated with a gas mixture containing oxygen and hydrogen just before graphene growth, at relatively

[a]*Materials Science and Engineering Program, University of California, Riverside, CA 92521, USA. E-mail: cozkan@engr.ucr.edu*

[b]*Department of Electrical and Computer Engineering, University of California, Riverside, CA 92521, USA*

[c]*Department of Chemical Engineering and Materials Science, University of Minnesota, Minneapolis, MN 55455, USA*

[d]*Department of Mechanical Engineering, University of California, Riverside, CA 92521, USA*

† These authors contributed equally to this work.

low temperature under near-atmospheric pressure. Our method is significantly different than the previously published work[27] in terms of the growth technique, experimental conditions including underlying substrate, temperature, and pressure, and overall material quality. We have performed CVD of POG films at a growth temperature of 800 °C, which is relatively lower than those for reported graphene (1000 °C)[14] and slightly oxidized graphene growths (1100 °C).[27] Detailed characterization of the films is performed using various microscopy and spectroscopy methods. We also provide a discussion concerning comparison of our results with other results obtained in the literature for GO and its derivatives.

Methods

Materials synthesis

Electropolishing of Cu foils. In a typical electropolishing experiment,[29] used as an anode, 25 μm thick Cu foil (99.8%) was electropolished in a homemade electrochemistry cell with a large and thick Cu foil as a cathode; the electropolishing solution was 1000 mL of deionized (DI) water, 500 mL of ortho-phosphoric acid (H_3PO_4), 500 mL of ethanol, 100 mL of isopropyl alcohol (IPA), and 10 g of urea. Supported by an alligator clip, the Cu foil was placed into the solution. A direct current (DC) power supply was used to apply 0.7 A of current at 4 V of potential for 90 s. After electropolishing, the Cu foil was rinsed with DI water, further washed with IPA, and then blow-dried with nitrogen.

CVD of POG films on Cu foils. In a typical CVD experiment, the electropolished Cu foils were inserted into a quartz tube, heated by a horizontal split-tube furnace. The quartz tube was initially pumped down to 1 mTorr to remove oxygen residue and then backed-filled with a gas mixture of argon (400 sccm) and hydrogen (100 sccm) to 700 Torr, which was maintained during the entire process. The quartz tube was then heated up to 800 °C (25 °C min^{-1}). Before the growth of the POG films, the Cu foils were preannealed at 800 °C for 3 min under oxygen (50 sccm) and hydrogen (100 sccm) gases. It should be noted that hydrogen (50 sccm) may interact with oxygen (100 sccm) to form a negligible amount of steam. A gas mixture of methane (200 sccm) and hydrogen (400 sccm) was used for the growth of the POG films at 800 °C for 5 min. After the growth, the system was slowly cooled down to room temperature (~40 °C min^{-1}) under hydrogen (100 sccm) and argon (400 sccm) gases.

Transfer of POG films from Cu foils to SiO_2/Si substrates and TEM grids. In a typical electrochemical delamination experiment,[29] a poly(methyl methacrylate) (PMMA) layer was first spin-coated on the POG/Cu samples as a capping layer. During the electrochemical delamination, DC voltage (1.8–2.2 V) is applied to the PMMA/POG/Cu as a cathode and a thick graphite rod as an anode in an aqueous solution of sodium hydroxide (NaOH) of 1 M. After the electrochemical delamination process, the PMMA/POG film was then fished out and transferred to a DI water bath to remove the solution reside. The PMMA/POG film was fished out on Si substrates with a 300 nm thick SiO_2 (SiO_2/Si) top layer and Quantifoil holey carbon transmission electron microscopy (TEM) grids. The PMMA layer was successively dissolved in acetone, followed by a IPA rinse and nitrogen blow.

Materials characterization

XPS and UPS characterization. X-ray photoelectron spectroscopy (XPS) and ultraviolet photoelectron spectroscopy (UPS) characterization were carried out using a Kratos AXIS ULTRADLD XPS system equipped with an Al Kα monochromated X-ray source, helium (He) I of ultraviolet (UV) source, and a 165 mm mean radius electron energy hemispherical analyzer. The size of slot for XPS is 300 μm × 700 μm, and the aperture for UPS has a diameter of 110 μm. The vacuum pressure was kept below 3×10^{-9} Torr, and the neutralizer was applied during the data acquisition. The XPS spectra were calibrated to the position of the carbon (C) sp^2 peak of 284.6 eV.

STEM and EELS analysis. An aberration-corrected (CEOS DCOR probe corrector) scanning transmission electron microscope (STEM) (FEI Titan G2 60-300) equipped with a Schottky extreme-field emission gun (X-FEG) and a monochromator was employed to analyze POG films transferred onto the holey carbon TEM grids. Electron energy loss spectroscopy (EELS) data was acquired using a Gatan Enfinium ER EEL Spectrometer.

Additional characterizations. Microstructural analyses were done by a FEI NNS450 scanning electron microscopy (SEM). Raman spectra were collected using a Horiba system with a 532 nm excitation laser (<2 mW excitation power, 100× objective lens). Thickness measurements were performed using Veeco Dimension 5000 atomic force microscopy (AFM) in non-contact mode.

Results and discussion

As described in Methods, we grew a POG film on an electropolished polycrystalline Cu foil at relatively low temperature under near-atmospheric pressure via CVD with help of oxygen. We then transferred the film (~1 cm × 1 cm) onto a SiO_2/Si substrate via the electrochemical delamination method (see Methods for details), as seen in Fig. 1a, and checked under optical microscopy and AFM.

Fig. 1b represents the optical microscopy image of the POG film on the SiO_2/Si substrate. The POG film with contrast is visible and can be easily distinguished from the substrate, similar to the case of GO,[30] graphene[31] and other 2D materials[17,32] on SiO_2/Si, due to the interference effects.[33–35] It appears that the POG film has a flat, smooth, transparent, and sheet-like surface with no observable pits or defects, except that the deformations including folds and wrinkles are formed at its edge possibly during the transfer process.

AFM in non-contact mode was employed to measure the thickness of the POG film. A typical high-resolution AFM topographic image acquired for region surrounding the edge of the POG film on the SiO_2/Si substrate is shown in Fig. 1c. Inset shows the height profile along the dashed lines. The height profile clearly shows that the edge of the film has a thickness of 1.33 nm, which is close to the thickness of monolayer GO reported by Mkhoyan et al.[10] The large edge step in the height profile can be attributed to the PMMA reside introduced during the transfer process since the dangling bonds at the edges of
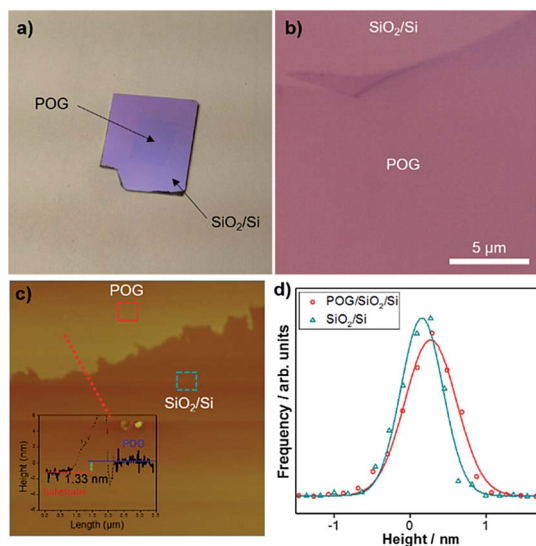
Fig. 1 Surface morphology of POG films. Digital photo (a) and optical microscopy (b) image of a CVD-grown POG film ($\sim$1 cm $\times$ 1 cm) transferred onto a SiO$_2$/Si substrate *via* electrochemical delamination method. (c) High resolution AFM topography image of a boundary between the POG film and the SiO$_2$/Si substrate. Inset shows the height profile along the dashed lines. (d) Comparison of the height histograms for the POG film on the SiO$_2$/Si substrate (open red circles) and the SiO$_2$/Si substrate (open dark cyan triangles). The data, corresponding to the regions designated by the dashed red and dark cyan squares (200 nm $\times$ 200 nm) in (c), are described by Gaussian distributions (solid lines) with standard deviations σ of 0.33 nm, and 0.27 nm, respectively. The height data was obtained by subtracting the mean value of the raw data, which allows the peak to be aligned in the middle.

POG films are attractive to the PMMA molecules, which are difficult to remove by acetone and IPA.

We also examined the surface roughness of the POG film and compared it with the underlying SiO$_2$/Si substrate by constructing the height histograms and calculating the standard deviations σ of these distributions from the high-resolution AFM topographic image in Fig. 1c. These histograms could be fit well by single Gaussian functions.[36,37] Fig. 1d compares the corresponding height histograms for the POG film and SiO$_2$/Si substrate surfaces, which are measured in squares (200 nm $\times$ 200 nm) in Fig. 1c. The histograms are described by Gaussian distributions with the standard deviations σ 0.33 nm and 0.27 nm, respectively, for the POG film on the SiO$_2$/Si substrate, and the bare SiO$_2$/Si substrate. Both curves are almost similar to each other, indicating that the POG film surface largely follows the underlying substrate morphology. The carbon-oxygen bonds and oxygen bonds alone can be also responsible for the surface roughness of the POG film.[10] The surface roughness of the POG film on the SiO$_2$/Si substrate is comparable to that of GO on a SiO$_2$/Si substrate.[10]

To check for the chemical composition, we transferred POG films onto a holey carbon TEM grid *via* an electrochemical delamination method, as described in Methods, and characterized with high angle annular dark-field (HAADF)-STEM imaging and energy-dispersive X-ray spectroscopy (EDX)

mappings. These measurements provide information on the elemental distribution at the atomic scale.[38] Fig. 2a shows an HAADF-STEM image of a POG film suspended over a hole ($\sim$1 μm) of the TEM grid. It is likely that the POG film was folded during the transfer onto the grid.[39] The small particles of high intensity (bright white) dispersed throughout the film are copper-oxide particles as determined by EDX elemental mapping in Fig. 2b. The copper-oxide particles over the film were most likely formed during the growth.[14] The Cu signal outside of the particles are mainly secondary signals originating from the Cu grid bars holding the TEM grid together. The presence of carbon and oxygen in the POG film was confirmed by STEM-EDX elemental mappings in Fig. 2c and d, respectively.

We studied the atomic and electronic structure of POG films using ADF-STEM imaging and EELS for measuring the fine structure of carbon and oxygen K-edges in a STEM. Fig. 3a shows a low magnification ADF-STEM image of a POG film. We collected SAED patterns in two different regions on the ADF image. Fig. 3b contains a SAED pattern collected from a monolayer region of the POG film. The SAED pattern shows that the structure of the film is hexagonal with a basal plane lattice parameter of $a = 2.45 \pm 0.05$ Å which is characteristic of graphene[40] and GO.[41] This hexagonal structure is also evident in Fig. 3c, which contains a SAED pattern collected from a region of two overlapping POG monolayer films. The overlap creates two sets of hexagonal diffraction spots in the SAED pattern that are rotated by an amount equivalent to the actual offset of the POG films, which, in this case, is about 20%.

In order to distinguish the POG film from graphene or graphite, EELS data of carbon and oxygen K-edge were collected
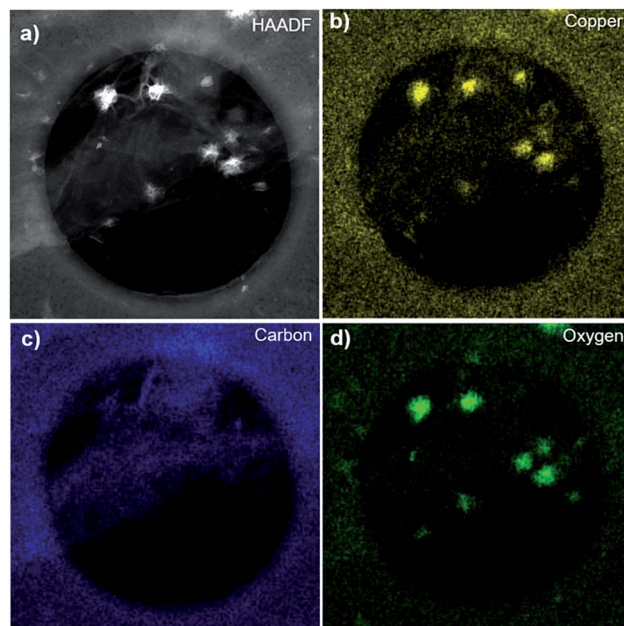

Fig. 2 Chemical composition of POG films. HAADF-STEM image (a) and corresponding Cu (b), carbon (c) and oxygen (d) elemental mappings of the POG film suspended over a holey carbon TEM grid collected using STEM-EDX. The diameter of the hole of the grid is $\sim$1 μm.
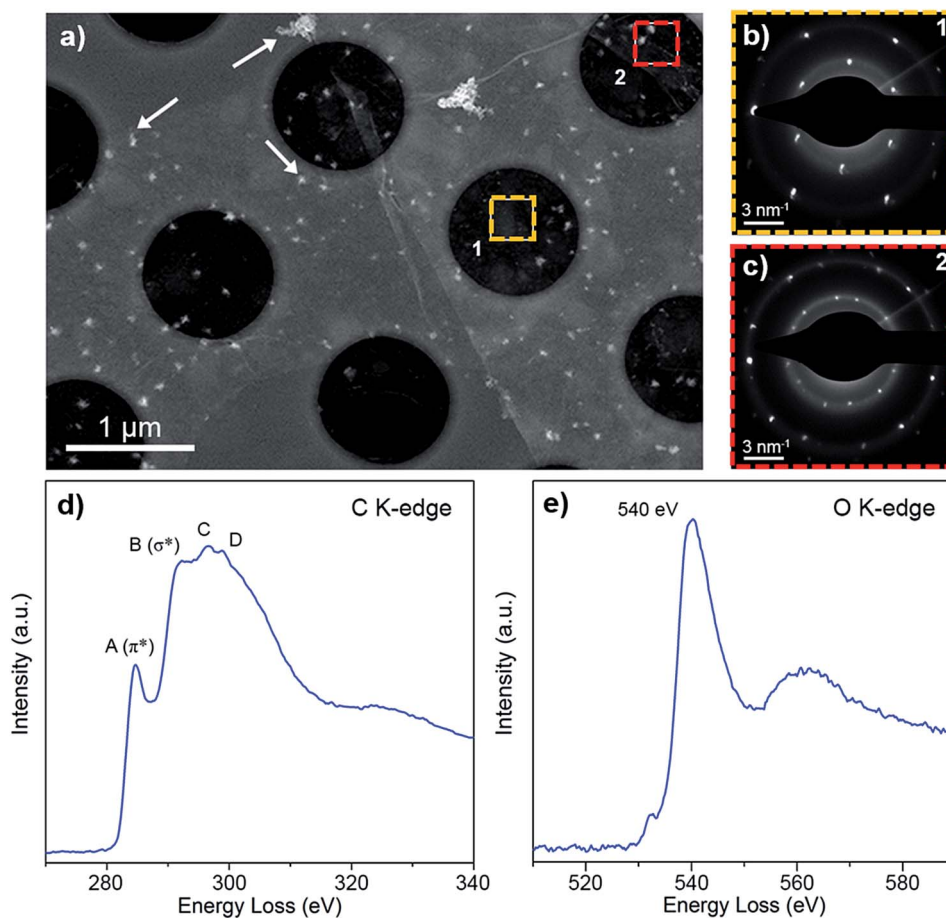
Fig. 3 Atomic and electronic structure of POG films. Low magnification ADF-STEM image (a) of a POG film on a holey carbon TEM grid. Arrows indicate copper-oxide particles detected on the POG film. SAED pattern from a single (b) and two overlapping (c) POG films. The locations of SAED pattern acquisition are indicated by square boxes in panel (a). EELS spectra of the C K-edge (d) showing signature GO fine structure, and the O K-edge (e).

as shown in Fig. 3d and e, respectively. The energies and relative intensities of the peaks in the fine structure of carbon (C) K-edge (features A to D) are consistent with previous EELS measurements of GO reported in literature.[10] This fine structure is unique to GO and is distinguishable from that of graphene and graphite.[10] The presence of oxygen in the films is further supported by a clear oxygen (O) K-edge EELS signal. Its peak onset at 530 eV and its maximum at 540 eV are consistent to a previous report.[10] It is worth mentioning that we also detected graphene and graphite regions in the POG film during STEM-EELS measurements.

Raman spectroscopy has proven to be highly useful as a non-invasive technique in the structural characterization of graphene and its derivatives.[42–45] Herein, we used Raman spectroscopy to identify POG films using a 532 nm excitation laser. The excitation power was kept at 2 mW to avoid local heating. Fig. 4a represents the optical microcopy image of a POG film, where Raman spectra was collected. The Raman spectra of the POG film consist of prominent D and G peaks, and weak 2D and D + G peaks in Fig. 4b. These features are similar to those seen GO[1,7,46] and its derivatives,[47–49] but deviate from those of graphene, where the D peak is absent or small, and the other peaks

are more clearly defined.[44,50] The G peak at around 1616 cm^{-1} is due to the bond stretching of all pairs of sp^2 atoms in both rings and chains.[44,51–53] The D peak at around 1355 cm^{-1} is due to the breathing modes of sp^2 atoms in rings,[44,52,54] which originates from the structural imperfections created by the attachment of oxygen functional groups on carbon atoms.[55] Generally, the intensity ratio of the D and G peaks (I_D/I_G) indicates the degree of disorder and oxygenation in a sp^3/sp^2 hybrid network of carbon atoms.[56–60] We calculated an I_D/I_G ratio of ~1.06 for the POG film, which is comparable to that of the POG sheets reported by Goki Eda et al.[48] The size of the defect-free sp^2 carbon clusters, L_a,[53,54] was estimated to be ~9.8 nm for the POG film, which is greater than that of GO reported in the literature,[48,61] consistent with the low oxygen content and low defect density. The overtone of the D peak, called 2D peak, appears around 2688 cm^{-1} is due to double resonance transitions resulting in production of two phonons with opposite momentum.[44] The low intensity and broad shape of the 2D peak is attributed to breaking of stacking order associated with oxidation reaction.[62,63] The disorder-induced combination mode of G and D bands,[64–66] called D + G peak (also known as D + D' peak), appears around 2942 cm^{-1}. The intensity ratio of the 2D and
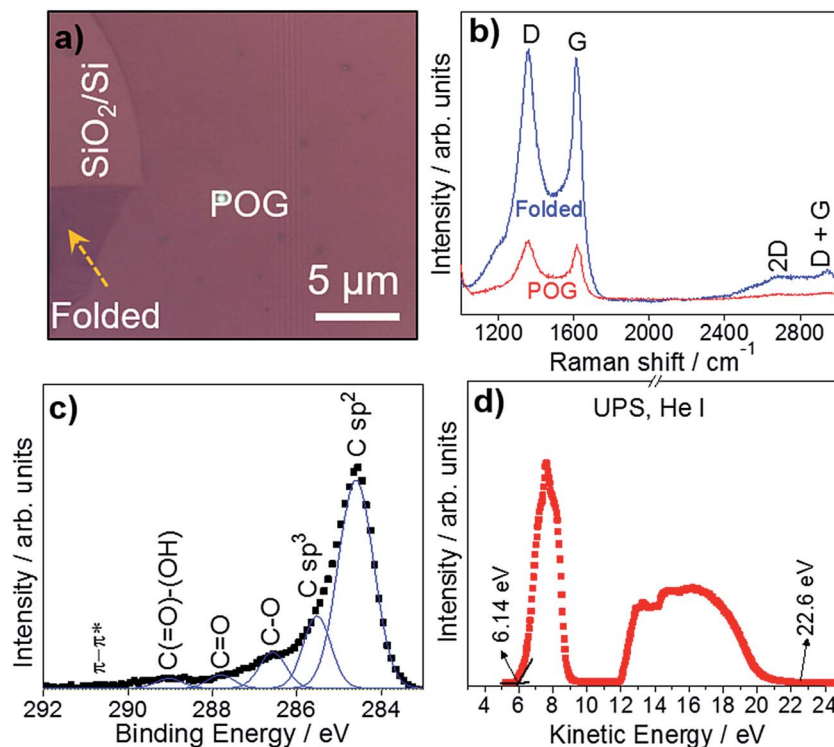
Fig. 4 Chemical and electronic properties of POG films. (a) The optical microscopy image of a POG film where Raman spectra were collected. (b) Raman spectra collected from the non-folded and folded regions of the POG film. (b and c) The C 1s region of the XPS spectra for the POG film. The spectra were deconvoluted to 6 components as described in the text. (d) Work functions of the POG film determined by UPS measurements with He I ($h\nu$ = 21.2 eV) source.

D + G peaks (I_{2D}/I_{D+G}) can be associated with defect density and oxygen content in GO and its derivatives.[58,62] This ratio is relatively low in the POG film, compare to that of GO,[48] indicating the low defect concentration in the POG film accompanied by a lower oxygen content.[58,62] We obtained Raman spectra for different spots of the POG film, and did not see a significant difference in the spectra. We also examined the effect of the folding on the Raman spectra of the POG film. The Raman spectra of the unfolded and folded parts of the POG film are represented in Fig. 4a, both of which was measured under the same experimental conditions. It is observed from the Raman spectra that folding gives rise to a significant increase in the intensities of the Raman peaks, suggesting that Raman signal is proportional to thickness of the film. In addition, no obvious shift position shift is observed in the Raman bands.

XPS, a surface sensitive technique, provides information on the surface chemistry of materials being analyzed.[18,67] XPS revealed the nature of the carbon bonds present in POG films. Fig. 4c shows the C 1s region of the XPS spectra for the POG film. After a Shirley background subtraction,[68] the high-resolution C 1s peak region of the XPS spectra was deconvoluted to the components, which are expected to be present in the film,[48,69,70] using Gaussian function. The deconvoluted C 1s peak region mainly consists of C sp^2, C sp^3, C–O, C=O, C(=O)–(OH) and π–π* at 284.60, 285.52, 286.57, 287.80, 289.03, and 290.72 eV, respectively, which consistent with the literature.[48,58,71] The majority of carbon atoms in the POG film has the

sp^2 hybridization, originating from unoxidized carbon atoms.[49] The weaker sp^3 hybridization of carbon atoms is due to the formation of covalent bonds during the oxidation.[49] The peak intensity ratio of oxygenated carbon peaks and non-oxygenated carbon peaks reflects the oxidation degree of the films.[59,72,73] In contrast to GO,[11,48] the peak intensity of oxygenated groups of the POG film is much weaker than that of non-oxygenated carbon peaks, suggesting that the POG is partially oxidized,[58,74] which is in good agreement with our Raman results. For the POG film, we found the oxygen content to be ~4.3%.

We also calculated the work function of POG films by UPS using excitation energy of 21.20 eV. Fig. 4d exhibits the UPS spectra of the POG film. From the UPS spectra, the work function was estimated as the energy level difference between the inelastic cutoff and the Fermi edge.[75] The calculated work function of the POG film is Φ = 4.74 eV, which is comparable to that of reduced graphene oxide (rGO),[75,76] but much higher than that of graphene.[77]

Conclusions

We have demonstrated a CVD method to grow POG films under near atmospheric pressure at reduced temperatures. The work reported here can be considered as a first step to growing the oxidized graphene films by CVD. We comprehensively characterize the films to establish unambiguously the fundamental

properties using several spectroscopy and microscopy methods. The presence of oxygen with low concentration in the graphene films was confirmed by spectroscopic characterization. The atomic and electronic structure of the POG films was revealed by STEM-EELS analysis. Our results offer a promising route towards the growth of oxidized graphene films with controllable oxygen concentration, which could be useful in various types of basic and applied research on GO based materials.

Acknowledgements

References

1 Y. Zhu, S. Murali, W. Cai, X. Li, J. W. Suk, J. R. Potts and R. S. Ruoff, *Adv. Mater.*, 2010, **22**, 3906.

2 D. R. Dreyer, A. D. Todd and C. W. Bielawski, *Chem. Soc. Rev.*, 2014, **43**, 5288.

3 A. Ganguly, S. Sharma, P. Papakonstantinou and J. Hamilton, *J. Phys. Chem. C*, 2011, **115**, 17009.

4 L. Staudenmaier, *Ber. Dtsch. Chem. Ges.*, 1898, **31**, 1481.

5 U. Hofmann and R. Holst, *Ber. Dtsch. Chem. Ges.*, 1939, **72**, 754.

6 W. S. Hummers and R. E. Offeman, *J. Am. Chem. Soc.*, 1958, **80**, 1339.

7 D. C. Marcano, D. V. Kosynkin, J. M. Berlin, A. Sinitskii, Z. Sun, A. Slesarev, L. B. Alemany, W. Lu and J. M. Tour, *ACS Nano*, 2010, **4**, 4806.

8 Y. L. Zhong, Z. Tian, G. P. Simon and D. Li, *Mater. Today*, 2015, **18**, 73.

9 A. J. Dhifaf, L. Neus and K. Kostas, *2D Mater.*, 2016, **3**, 14006.

10 K. A. Mkhoyan, A. W. Contryman, J. Silcox, D. A. Stewart, G. Ed, C. Mattevi, S. Miller and M. Chhowalla, *Nano Lett.*, 2009, **9**, 1058.

11 D. R. Dreyer, S. Park, C. W. Bielawski and R. S. Ruoff, *Chem. Soc. Rev.*, 2010, **39**, 228.

12 A. Nourbakhsh, M. Cantoro, T. Vosch, G. Pourtois, F. Clemente, M. H. V. D. Veen, J. Hofkens, M. M. Heyns, S. D. Gendt and B. F. Sels, *Nanotechnology*, 2010, **21**, 435203.

13 T. Gokus, R. R. Nair, A. Bonetti, M. Böhmler, A. Lombardo, K. S. Novoselov, A. K. Geim, A. C. Ferrari and A. Hartschuh, *ACS Nano*, 2009, **3**, 3963.

14 I. Ruiz, W. Wang, A. George, C. S. Ozkan and M. Ozkan, *Adv. Sci., Eng. Med.*, 2014, **6**, 1070.

15 Z. Mutlu, R. J. Wu, D. Wickramaratne, S. Shahrezaei, C. Liu, S. Temiz, A. Patalano, M. Ozkan, R. K. Lake, K. A. Mkhoyan and C. S. Ozkan, *Small*, 2016, **12**, 2998.

16 Z. Mutlu, D. Wickramaratne, S. Turkyilmaz, H. H. Bay, Z. Favors, M. Ozkan, R. Lake and C. Ozkan, *J. Nanosci. Nanotechnol.*, 2017, **16**, 8419.

17 Z. Mutlu, M. Ozkan and C. S. Ozkan, *Mater. Chem. Phys.*, 2016, **176**, 52.

18 Z. Mutlu, S. Shahrezaei, S. Temiz, M. Ozkan and C. S. Ozkan, *J. Electron. Mater.*, 2016, **45**, 2115.

19 O. V. Yazyev and S. G. Louie, *Nat. Mater.*, 2010, **9**, 806.

20 C. S. R. Vargas, H. L. Zhuang, P. Y. Huang, A. M. V. D. Zande, S. Garg, P. L. Mceuen, D. A. Muller, R. G. Hennig and J. Park, *Nano Lett.*, 2011, **11**, 2259.

21 Y. Hao, M. S. Bharathi, L. Wang, Y. Liu, H. Chen, S. Nie, X. Wang, H. Chou, C. Tan, B. Fallahazad, H. Ramanarayan, C. W. Magnuson, E. Tutuc, B. I. Yakobson, K. F. McCarty, Y. W. Zhang, P. Kim, J. Hone, L. Colombo and R. S. Ruoff, *Science*, 2013, **342**, 720.

22 C. W. Magnuson, X. Kong, H. Ji, C. Tan, H. Li, R. Piner, C. A. Ventrice and R. S. Ruoff, *J. Mater. Res.*, 2014, **29**, 403.

23 Z. R. Robinson, E. W. Ong, T. R. Mowll, P. Tyagi, D. K. Gaskill, H. Geisler and C. A. Ventrice, *J. Phys. Chem. C*, 2013, **117**, 23919.

24 P. B. Weimer, B. Brennan, A. J. Pollard and S. Hofmann, *Chem. Mater.*, 2016, **28**, 8905.

25 R. J. Chang, C. H. Lee, M. K. Li, C. W. Chen and C. Y. Wen, *Nanoscale*, 2017, **9**, 2324–2329.

26 T. Liang, C. Luan, H. Chen and M. Xu, *Nanoscale*, 2017, **9**, 3719–3735.

27 R. U. R. Sagar, M. Namvari, S. T. Navale and F. J. Stadler, *J. Colloid Interface Sci.*, 2017, **490**, 844–849.

28 Y. Liu and Y. Chen, *J. Appl. Phys.*, 2016, **119**, 1–7.

29 Y. Wang, Y. Zheng, X. Xu, E. Dubuisson, Q. Bao, J. Lu and K. P. Loh, *ACS Nano*, 2011, **5**, 9927–9933.

30 I. Jung, J. S. Rhee, J. Y. Son, R. S. Ruoff and K. Y. Rhee, *Nanotechnology*, 2012, **23**, 25708.

31 S. P. Koenig, N. G. Boddeti, M. L. Dunn and J. S. Bunch, *Nat. Nanotechnol.*, 2011, **6**, 543–546.

32 R. Ionescu, W. Wang, Y. Chai, Z. Mutlu, I. Ruiz, Z. Favors, D. Wickramaratne, M. Neupane, L. Zavala, R. Lake, M. Ozkan and C. S. Ozkan, *IEEE Trans. Nanotechnol.*, 2014, **13**, 749–754.

33 S. Roddaro, P. Pingue, V. Piazza, V. Pellegrini and F. Beltram, *Nano Lett.*, 2007, **7**, 2707–2710.

34 P. Blake, E. W. Hill, A. H. C. Neto, K. S. Novoselov, D. Jiang, R. Yang, T. J. Booth and A. K. Gei, *Appl. Phys. Lett.*, 2007, **91**, 063124.

35 A. Reina, X. Jia, J. Ho, D. Nezich, H. Son, V. Bulovic, M. S. Dresselhaus and J. Kong, *Nano Lett.*, 2009, **9**, 30–35.

36 S. Hwang, H. Seo, D. C. Jeong, L. Wen, J. G. Han, C. Song and Y. Kim, *Sci. Rep.*, 2015, **5**, 11201.

37 C. H. Lui, L. Liu, K. F. Mak, G. W. Flynn and T. F. Heinz, *Nature*, 2009, **462**, 339–341.

38 J. S. Jeong, M. L. Odlyzko, P. Xu, B. Jalan and K. A. Mkhoyan, *Phys. Rev. B*, 2016, **93**, 165140.

39 J. R. Kyle, C. S. Ozkan and M. Ozkan, *Nanoscale*, 2012, **4**, 3807–3819.

40 J. C. Meyer, A. K. Geim, M. I. Katsnelson, K. S. Novoselov, T. J. Booth and S. Roth, *Nature*, 2007, **446**, 60–63.

41 N. R. Wilson, P. A. Pandey, R. Beanland, R. J. Young, I. A. Kinloch, L. Gong, Z. Liu, K. Suenaga, J. P. Rourke, S. J. York and J. Sloan, *ACS Nano*, 2009, **3**, 2547–2556.

42 A. C. Ferrari, J. C. Meyer, V. Scardaci, C. Casiraghi, M. Lazzeri, F. Mauri, S. Piscanec, D. Jiang, K. S. Novoselov, S. Roth and A. K. Geim, *Phys. Rev. Lett.*, 2016, **97**, 187401.

43 A. C. Ferrari and D. M. Basko, *Nat. Nanotechnol.*, 2013, **8**, 235–246.

44 A. C. Ferrari, *Solid State Commun.*, 2007, **143**, 47–57.

45 C. Liu, C. Li, K. Ahmed, Z. Mutlu, C. S. Ozkan and M. Ozkan, *Sci. Rep.*, 2016, **6**, 29183.

46 K. N. Kudin, B. Ozbas, H. C. Schniepp, R. K. Prud'homme, I. A. Aksay and R. Car, *Nano Lett.*, 2008, **8**, 36–41.

47 I. K. Moon, J. Lee, R. S. Ruoff and H. Lee, *Nat. Commun.*, 2010, **1**, 73.

48 G. Eda, J. Ball, C. Mattevi, M. Acik, L. Artiglia, G. Granozzi, Y. Chabal, T. D. Anthopoulos and M. Chhowalla, *J. Mater. Chem.*, 2011, **21**, 11217.

49 S. Abdolhosseinzadeh, H. Asgharzadeh and H. Seop Kim, *Sci. Rep.*, 2015, **5**, 10160.

50 J. K. Reiber, A. Guvenc, W. Wang, M. Ghazinejad, J. Lin, S. Guo, C. S. Ozkan and M. Ozkan, *Small*, 2011, **7**, 2599–2606.

51 A. C. Ferrari and J. Robertson, *Phys. Rev. B: Condens. Matter Mater. Phys.*, 2001, **64**, 75414.

52 L. M. Malard, M. A. Pimenta, G. Dresselhaus and M. S. Dresselhaus, *Phys. Rep.*, 2009, **473**, 51–87.

53 I. Childres, L. Jauregui, W. Park, H. Cao and Y. Chen, *New Dev. Photon Mater. Res.*, 2013, 1–20.

54 L. G. Cançado, A. Jorio, E. H. Ferreira, F. Stavale, C. A. Achete, R. B. Capaz, M. V. O. Moutinho, A. Lombardo, T. Kulmala and A. C. Ferrari, *Nano Lett.*, 2011, **11**, 3190–3196.

55 D. Chen, H. Feng and J. Li, *Chem. Rev.*, 2012, **112**, 6027–6053.

56 S. Eigler, C. Dotzer and A. Hirsch, *Carbon*, 2012, **50**, 3666–3673.

57 S. Pei and H. M. Cheng, *Carbon*, 2012, **50**, 3210–3228.

58 Y. Xu, K. Sheng, C. Li and G. Shi, *J. Mater. Chem.*, 2011, **21**, 7376.

59 G. Sobon, J. Sotor, J. Jagiello, R. Kozinski, M. Zdrojek, M. Holdynski, P. Paletko, J. Boguslawski, L. Lipinska and K. M. Abramski, *Opt. Express*, 2012, **20**, 19463.

60 K. Vijayarangamuthu, S. Ahn, H. Seo, S. H. Yoon, C. M. Park and K. J. Jeon, *Adv. Mater.*, 2016, **28**, 661–667.

61 K. Erickson, R. Erni, Z. Lee, N. Alem, W. Gannett and A. Zettl, *Adv. Mater.*, 2010, **22**, 4467–4472.

62 H. Wang, J. T. Robinson, X. Li and H. Dai, *J. Am. Chem. Soc.*, 2009, **131**, 9910–9911.

63 K. Krishnamoorthy, M. Veerapandian, K. Yun and S. J. Kim, *Carbon*, 2013, **53**, 38–49.

64 J. C. Delgado, J. M. R. Herrera, X. Jia, D. A. Cullen, H. Muramatsu, Y. A. Kim, T. Hayashi, Z. Ren, D. J. Smith, Y. Okuno, T. Ohba, H. Kanoh, K. Kaneko, M. Endo, H. Terrones, M. S. Dresselhaus and M. Terrones, *Nano Lett.*, 2008, **8**, 2773–2778.

65 C.-Y. Su, Y. Xu, W. Zhang, J. Zhao, X. Tang, C. H. Tsai and L. J. Li, *Chem. Mater.*, 2009, **21**, 5674–5680.

66 Y. Kawashima and G. Katagiri, *Phys. Rev. B: Condens. Matter Mater. Phys.*, 1995, **52**, 10053–10059.

67 C. Li, C. Liu, W. Wang, Z. Mutlu, J. Bell, K. Ahmed, R. Ye, M. Ozkan and C. S. Ozkan, *Sci. Rep.*, 2017, **7**, 917.

68 D. A. Shirley, *Phys. Rev. B: Condens. Matter Mater. Phys.*, 1972, **5**, 4709–4714.

69 C. Mattevi, G. Eda, S. Agnoli, S. Miller, K. A. Mkhoyan, O. Celik, D. Mastrogiovanni, G. Granozzi, E. Garfunkel and M. Chhowalla, *Adv. Funct. Mater.*, 2009, **19**, 2577–2583.

70 D. Yang, A. Velamakanni, G. Bozoklu, S. Park, M. Stoller, R. D. Piner, S. Stankovich, I. Jung, D. A. Field, C. A. Ventrice and R. S. Ruoff, *Carbon*, 2009, **1**, 145–152.

71 R. U. R. Sagar, M. Namvari, S. T. Navale and F. J. Stadler, *J. Colloid Interface Sci.*, 2017, **490**, 844–849.

72 D. Mhamane, V. Aravindan, M. S. Kim, H. K. Kim, K. C. Roh, D. Ruan, S. H. Lee, M. Srinivasan and K. B. Kim, *J. Mater. Chem. A*, 2016, **15**, 5578–5591.

73 J. Chen, Y. Zhang, M. Zhang, B. Yao, Y. Li, L. Huang, C. Li and G. Shi, *Chem. Sci.*, 2015, **7**, 1–18.

74 R. U. R. Sagar, M. Namvari, S. T. Navale and F. J. Stadler, *J. Colloid Interface Sci.*, 2017, **490**, 844–849.

75 G. Jun, G. Hoon, S. H. Jin, B. Lee, B. H. Kim, W. S. Chae, S. H. Hong and S. Jeon, *Energy Environ. Sci.*, 2013, **6**, 3000.

76 L. Sygellou, G. Paterakis, C. Galiotis and D. Tasis, *J. Phys. Chem. C*, 2016, **120**, 281–290.

77 R. Garg, N. Dutta and N. Choudhury, *Nanomaterials*, 2014, **4**, 267–300.